

## Analysis of damages on induction motors by the finite element method

Damian Mazur

Rzeszów University of Technology, ul. W. Pola 2, 35-959 Rzeszów, Poland

(Received November 3, 1999)

The results of computations of forces and moments in induction motor made with OPERA 2D program and possibilities of application of FEA methods to consider the failure states during the calculations of induction machine dynamics are discussed in this paper. A mathematics model of an induction motor makes it possible to perform the calculations and analysis of stator currents and electromagnetic torque when the rotor rotates eccentrically, as well as when a bar or rotor ring is broken. A tool has been created which enables to predict preliminarily the results of the defects, which might be introduced at the motor manufacturing stage. To calculate 3D free vibration frequencies of the rotor system of the motor under consideration the PATRAN package has been used. It allowed us to examine the resonance frequencies of the rotor. For the diagnostic measurements the MotorMonitor™ program has been applied. It was possible to attain high computational effectiveness due to parallel programming on CONVEX computers of ACC "CYFRONET".

### 1. INTRODUCTION

The cage rotor asynchronous motors are of simple design, and are used generally in uncontrolled drives. Because of their multitude and total installed power, they play a dominant role in the industry. When powered by frequency converters, they may be also useful in continuous speed regulation. For this purpose the ring rotor motors are applied, too. In order to get a wide range of regulation if we require an increased electromagnetic moment at start-up, overload and coasting, DC motors used among the others. They are also powered by thyristor current converters. So the asynchronous and commutator motors complement each other. They are principal types of motors used in the industry [5, 6, 16].

Fast and effective computational methods, which allow for the examination of the operation of these motors at dynamic states (particularly when the operational requirements are increased) are necessary. When forming the model, it is indispensable to avoid any additional simplifications. It would be an ideal situation if the model data were obtained from a motor project without any modifications.

The analysis of the dynamic properties of the electric motors had been based – through the long period of their development – on the model which included the main spatial harmonic of the magnetic field, i.e. so called a monoharmonic model. The new period in the field of testing and modeling of electric motors has been started at the breakthrough in the computer techniques. With these we are capable to perform a numerical analysis of complex polyharmonic model of an electric motor, so that the model would include the spatial harmonics of the magnetic field in the airgap of higher order. These new capabilities made the interest in the above concept to grow considerably. We could get the optimum of the electromechanical conversion if the spatial distribution of the magnetic field along the motor circumference would have a sinusoidal pattern. In the reality the curve is being deformed and includes many higher harmonics [7, 15]. The source of these higher harmonics is as follows:

- a) non-sinusoidal spatial distribution of magnetomotive forces (MMF's) which occurs as the result of discrete distribution pattern of wires laid in the stator slots as well as bars in the rotor slots,
- b) nonuniform airgap length caused by the stator/rotor slotting,
- c) rotor eccentricity caused by motor manufacturing inaccuracies,
- d) magnetic circuit saturation.

The aim of this paper is, among the others, to tailor the model based on the FEA method to the calculations of stator currents and electromagnetic torque if simultaneously occur:

- broken cage bar, broken ring, broken bar and ring. They are simulated with the increase of gap resistance in bars and cage ring segments [11, 12, 13].
- rotor eccentricity, which can take the: static, dynamic or mixed form (Fig. 1):
  - a) **static eccentricity** occurs when the rotor is displaced in relation to the stator bore center, but still rotates around its axis. This could be caused by e.g. some displacement of the bearing seats. For the static eccentricity such displacement does not change with time. The source of this occurrence may be incorrect assembly or increased wear of bearings [1, 10].
  - b) **dynamic eccentricity** occurs when the rotor center does not overlay the center of rotation, and the minimum airgap rotates as the rotor rotates. This means that the dynamic eccentricity is a function of space and time. This occurs when the shaft is machined incorrectly in relation to the rotor center. When the bearings are placed correctly in the stator then the center of gravity of the rotor rotates in relation to the center of the rotation of the motor. The source of this occurrence can be; bending of the shaft, mechanical resonance at critical speeds, bearing wear [22].
  - c) **mixed eccentricity** appears when the both forms of the eccentricity occur simultaneously. This means that both center of rotation of the motor (i.e. shaft) and the rotor laminated core assembly are displaced in relation to the motor shaft.

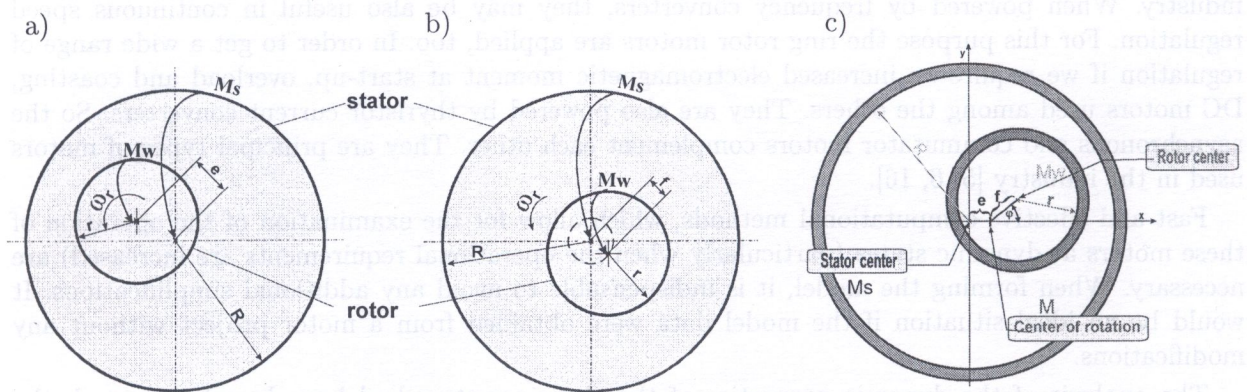


Fig. 1. Eccentricity forms under consideration; a) static eccentricity, b) dynamic eccentricity, c) mixed eccentricity

## 2. DESCRIPTION OF THE CIRCUMFERENTIAL-POLAR 2.5D MODEL BASED ON THE FINITE ELEMENTS METHOD

The model described in [4, 8, 9, 14, 21] was applied for the calculations. For the calculation of the currents and torques to time for the asynchronous motor type Sg90S-4 with aluminium cage

manufactured with "TAMEL" in Tarnów, Poland, presented previously method has been used. The output of the motor is  $P = 1.1$  kW, rated voltage is  $U_N = 380$  volts and rated current  $-I_N = 2.8$  amps, rated speed is  $n = 1415$  rpm, the stator slot quantity is 36 and the rotor slot quantity is 28. The computational program presented here has also produced spatial harmonics of radial forces and electromagnetic torque of higher order. For the detailed description of the model used in the calculations refer to [4, 8]. The skew of the bars is considered by the way of partitioning of the asynchronous machine into elementary machines having straight, but shifted bars (Fig. 2).

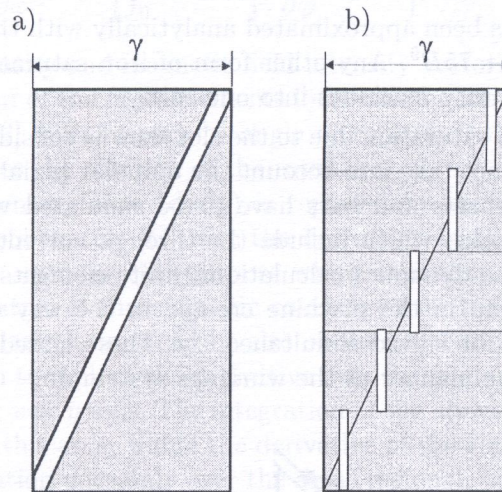


Fig. 2. Method of partitioning of the asynchronous machine into elementary machines; a) the rotor prior to the partitioning, b) the rotor after partitioning into elementary machines

We assume that the magnetic field is two-dimensional in each elementary machine. It is calculated with the finite elements method. This is why we are able to parallelize the calculations and perform the calculations for each elementary machine on a separate processor set. At the end of a time step, the elementary machines are integrated in one entity which is the electric motor under consideration with the equation sets for electric circuits. To consider the current displacement phenomenon in the rotor bars, we do the partitioning them into the partial bars.

Each bar is partitioned with planes parallel to the motor axis and to the bar base into partial bar (Fig. 3). The model did not include the magnetic field in the face regions. Thus it was necessary to supply the resistance and inductance data for the face dissipation of stator windings and the resistance of the partial bars  $R_{fpr}$ ,  $R_{fcz}$  and the dissipation inductance  $L_{fcz}$  of the ring segment.

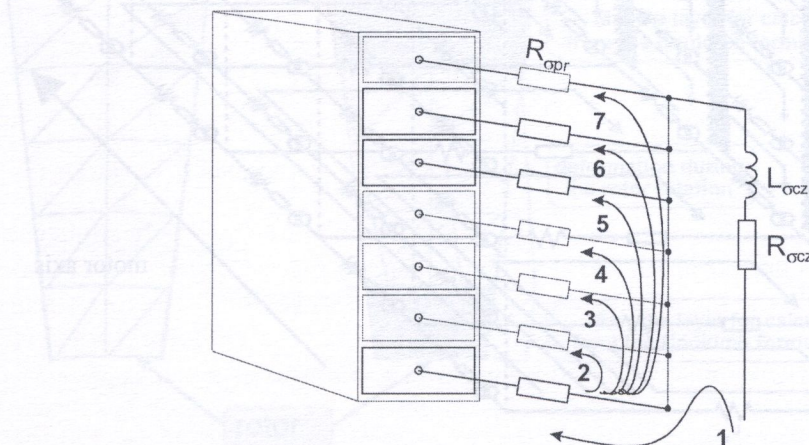


Fig. 3. Method of bar partitioning in the elementary machine into partial bars and forming the closed loops of electric circuits for the bar

These data can be obtained from the design calculations for the engine. The dissipation inductance of the partial bars due to slotting are included automatically within the program.

The current density in each partial bar was constant, but different in each partial bar being a part of same bar. These partial bars are linked to form one bar in section planes of each elementary machine, and in the rotor faces they are linked through the rings. The closed loop current  $i_o$  flows through each independent closed loop. Any current  $i_g$ , which flows through each single circuit branch, which are either stator windings or partial bars, can be expressed with these closed loop currents (Fig. 4).

The magnetization curve has been approximated analytically with the polynomial of 9-th order of the form  $H = 100B + 3B^3 + 75B^9$ . Any other form of iron saturation curve can be used. The winding set links all the elementary machines into one entity.

Thus the increase in the iron saturation due to the slot skew is considered automatically. Because the model presented here does not take into account the unipolar (axial) flux, the through currents, which flow between the core sheets and bars have to be simulated with substitute impedances. These can be RL ladder networks, which include the through current displacement phenomenon pretty well. To perform machine dynamics calculations, finite elements method equation system is formulated. For each closed loop in the machine created in the way described above, the closed loop current equations have to be solved simultaneously. These closed loop equations link all the elementary machine in the same manner as the windings system do.

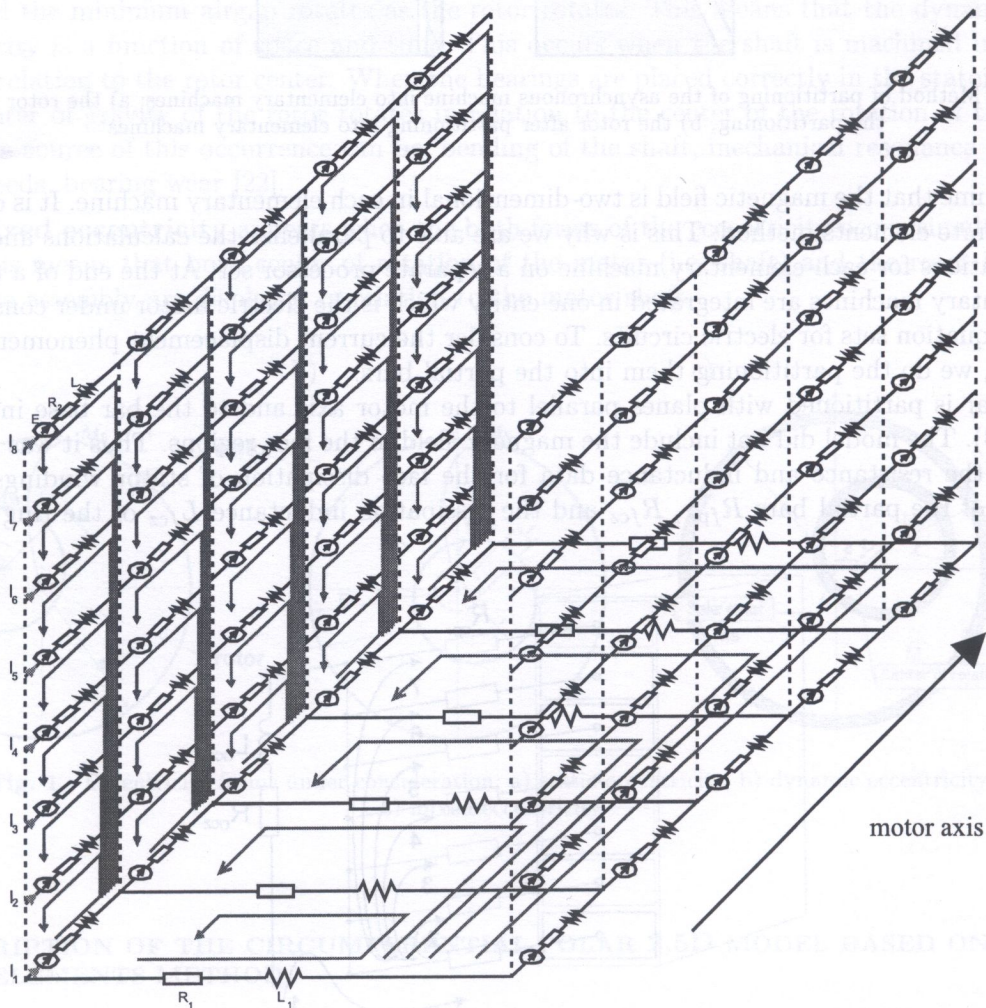


Fig. 4. Induction motor partitioning into 5 elementary machines with the planes straight to the motor axis  
- forming the closed loops for the rotor

### 3. CALCULATION OF ELECTROMAGNETIC TORQUE AND FORCES USING THE J.L. COULOMB METHOD WHEN DEFECTS ARE PRESENT

To calculate the forces and the electromagnetic torque in the machine with defects under consideration the J.L. Coulomb method [2, 3, 8] has been applied. The following formula (1) is used for this purpose,

$$M_{el} = \int_V \left\{ -B^T [G]^{-1} \frac{\partial [G]}{\partial \varphi} H + \left[ \int_0^H B dH \right] \frac{\partial |G|}{\partial \varphi} |G|^{-1} \right\} dV, \quad (1)$$

where  $B$  and  $H$  are flux density and magnetic field intensity vectors, respectively.  $[G]$  is the Jacobi matrix of the transformation of the finite elements local coordinate system into the global one. The derivative of this matrix  $[G]$  with respect to angle of rotation ( $\varphi$ ) stands for the finite elements deformation, which simulates the rotation of the rotor.

At integration the elementary area ( $dxdy$ ) is replaced by the product of  $|G|dudv$ , where  $|G|$  is a determiner of the Jacobi matrix  $[G]$ . For the derivation of the formula under consideration, see [2]. A relation has been used for this purpose which says that the electromagnetic torque can be obtained from the derivative of the magnetic co-energy over the angle of rotation assuming the constant currents. The similar relations can be also obtained for the  $F_x$  and  $F_y$  forces, which act on the rotor. It will suffice then to replace the derivative over the angle of rotation  $\varphi$  with the derivative over the displacement along  $x$  or  $y$ -axis. The integration of the above formula has to be performed in the global coordinates over this area, where the derivative of the Jacobi matrix is not equal to zero. This means that the integration goes only over the area (regions), which are subject to deformation at the rotor rotation. So the rotation of the rotor in the finite elements method must be considered in an appropriate way.

For the sake of the calculations, the airgap in the motor was divided into 5 layers, which helped to obtain a very good accuracy. It was assumed that at the rotor rotation only the layers 2 through 4 are being deformed, but the layer 1 (next to stator) and the 5 (next to rotor) retain unchanged form (Fig. 5).

If the angular displacement of the rotor is greater than the mesh discretization step, then the mesh deforms only by the fractional part of the quotient of the rotor angular displacement ( $\varphi$ ) by the element discretization step. Then the re-numbering of nodes of the rotor mesh by the integer part of this quotient follows.

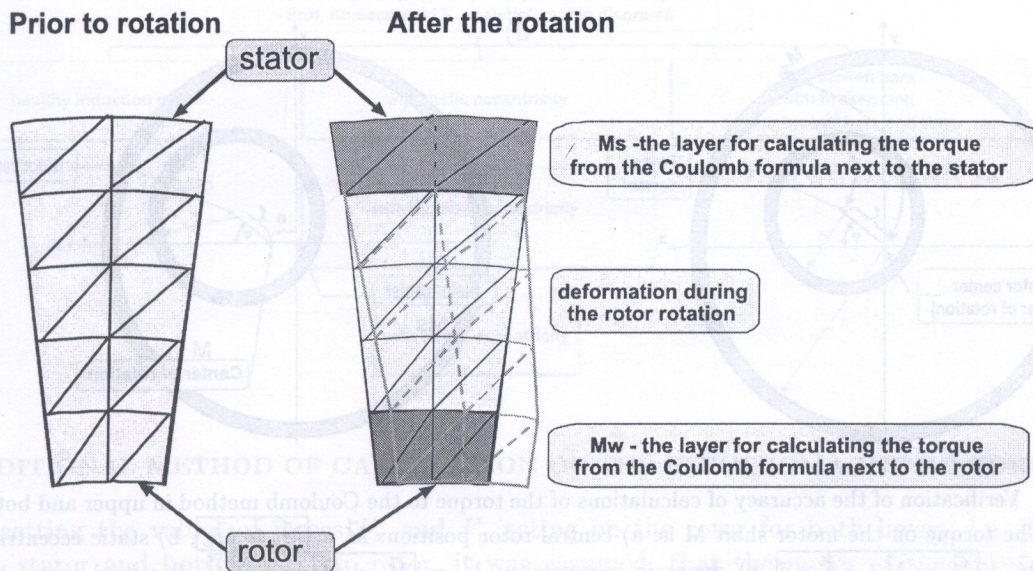
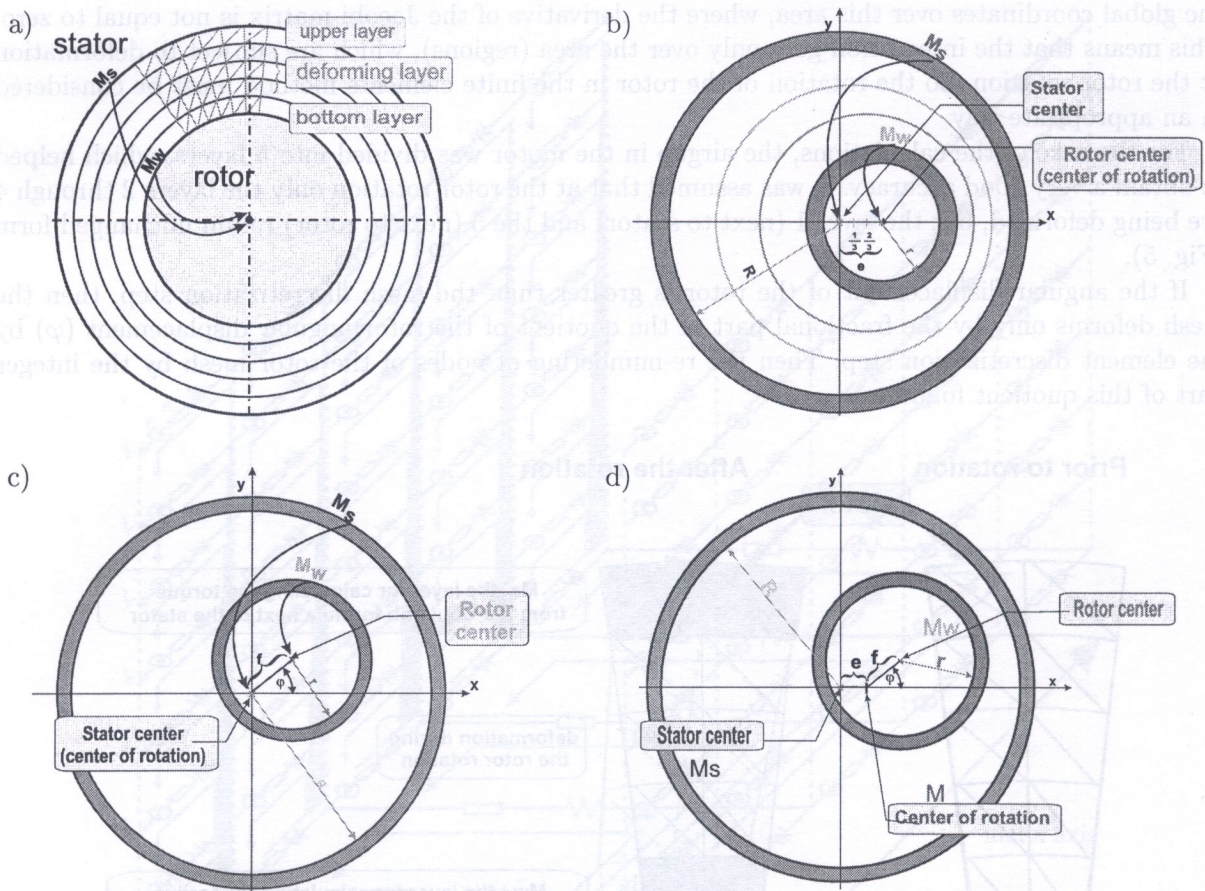


Fig. 5. Assumed deformation form of the finite elements layer within the airgap of the induction motor at the rotor rotation

When performing the calculations of the electromagnetic torque to the J.L. Coulomb formula either in the upper or the bottom layer it is necessary though to assume, that the rotor movement at large is reflected by the deformation of the layer being considered. In reality though, at the rotation, only three layers (2, 3, 4, i.e. between the layer next to stator and the layer next to rotor) are being deformed in the manner described above.

By performing test calculations of the electromagnetic torque (Fig. 6) it was verified that the electromagnetic torques calculated from the upper layer ( $M_s$ ) and the bottom one ( $M_w$ ), which are not subject to deformation during rotation, retain correct values when both the increase of the rotation angle matches the discretization step of the finite element mesh (i.e. the rotor “snaps” to the finite element discretization step) and with any rotor rotation angle. This does not make the mesh to deform in these layers and associated with it magnetic energy fluctuations, which is the source of errors. On the other hand a great influence to the form deformation of the elements have torques calculated in the middle layers. During this deformation we can say that the airgap length changes and obtained torque includes also the force effect, caused with this change.

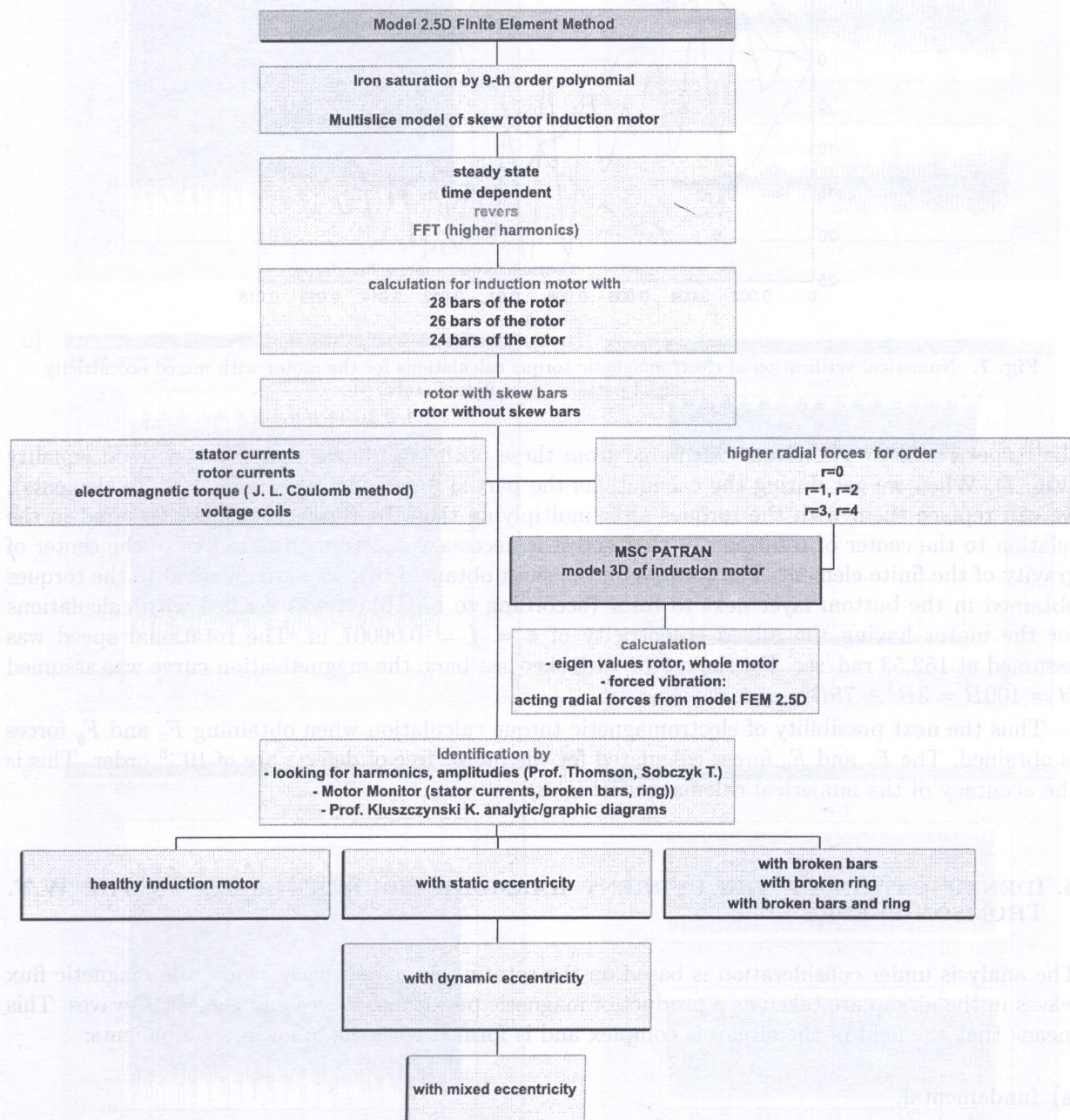
The elements in the upper and bottom layers of the airgap should be, in addition, placed so that to assure the minimum magnetic energy, calculated also in the context of their arrangement. So the possible deformation of these elements does not introduce any additional torque and the result is correct. It can be said that then the hypothetical derivative over the airgap length change in these layers (1 and 5) equals to zero.



**Fig. 6.** Verification of the accuracy of calculations of the torque to the Coulomb method in upper and bottom layer. The torque on the motor shaft  $M$  is: a) central rotor position:  $\vec{M} = [\vec{M}_s \cong \vec{M}_w]$ , b) static eccentricity:  $\vec{M} = \vec{M}_w$ ;  $[\vec{M}_s = \vec{M}_w - \vec{F} \times \vec{e}]$ , c) dynamic eccentricity:  $\vec{M} = [\vec{M}_s = \vec{M}_w - \vec{F} \times \vec{f}]$ , d) mixed eccentricity:  $\vec{M} = \vec{M}_s + \vec{F} \times \vec{e} = \vec{M}_w - \vec{F} \times \vec{f}$ , where  $e$  is the static eccentricity,  $f$  is the dynamic eccentricity and  $\varphi$  is the angle of rotation

For the calculations of the motor showing the rotor eccentricity, the  $M_w$  torque calculated from the finite element layer in the airgap placed next to the rotor was used the most frequently. this layer was moving with the rotor and was not deformed.

#### 4. ALGORITHM CALCULATION BY 2.5D FEM MODEL OF INDUCTION MOTOR



#### 5. ADDITIONAL METHOD OF CALCULATION OF THE ELECTROMAGNETIC TORQUE

When getting the values of forces  $F_x$  and  $F_y$  acting on the rotor for both layers, i.e. the upper next to stator and bottom next to rotor, it was assumed, that the nodes of the finite elements found close to the stator or rotor center are displaced along  $x$  or  $y$  axes respectively. We can say it corresponded to the displacement of the circle where these nodes were located in the direction of

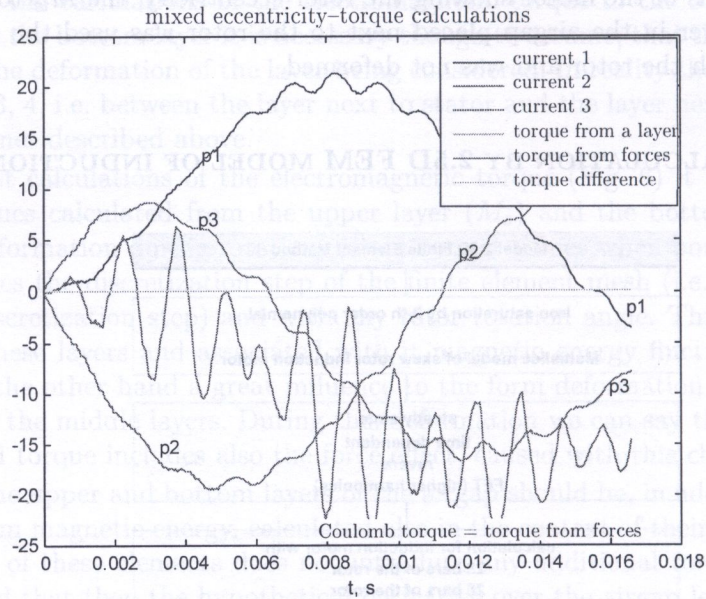


Fig. 7. Numerical verification of electromagnetic torque calculations for the motor with mixed eccentricity - initial pattern (transitional state)

the respective axis. The forces calculated from these both layers had shown a very good equality (Fig. 7). When we get during the calculations the partial forces (acting on single finite elements), we can replace them with the torques after multiplying them by respective radii measured in the relation to the center of rotation. To that end it is necessary to assume the radius to the center of gravity of the finite element. The torques on the shaft obtained this way are identical to the torques obtained in the bottom layer next to rotor (according to Fig. 6). It was verified with calculations for the motor having the mixed eccentricity of  $e = f = 0.00007$  m. The rotational speed was assumed at 152.53 rad/sec. For the motor with skewless bars, the magnetization curve was assumed  $H = 100B = 3B^3 + 75B^9$ .

Thus the next possibility of electromagnetic torque calculation when obtaining  $F_x$  and  $F_y$  forces is obtained. The  $F_x$  and  $F_y$  forces calculated for the motor free of defects are of  $10^{-8}$  order. This is the accuracy of the numerical calculations (Fig. 8).

## 6. IDENTIFICATION OF THE CURRENT HARMONIC SOURCES BASED ON THE W.T. THOMSON THEORY

The analysis under consideration is based on the rotating wave approach, where the magnetic flux waves in the airgap are taken as a product of magnetic permeance waves and the MMF waves. This means that the field in the airgap is complex and is formed with the following components:

- fundamental,
- stator and rotor MMF harmonics,
- stator and rotor magnetic permeance harmonics due to slotting,
- airgap eccentricity magnetic permeance harmonics,
- magnetic permeance harmonics due to saturation.



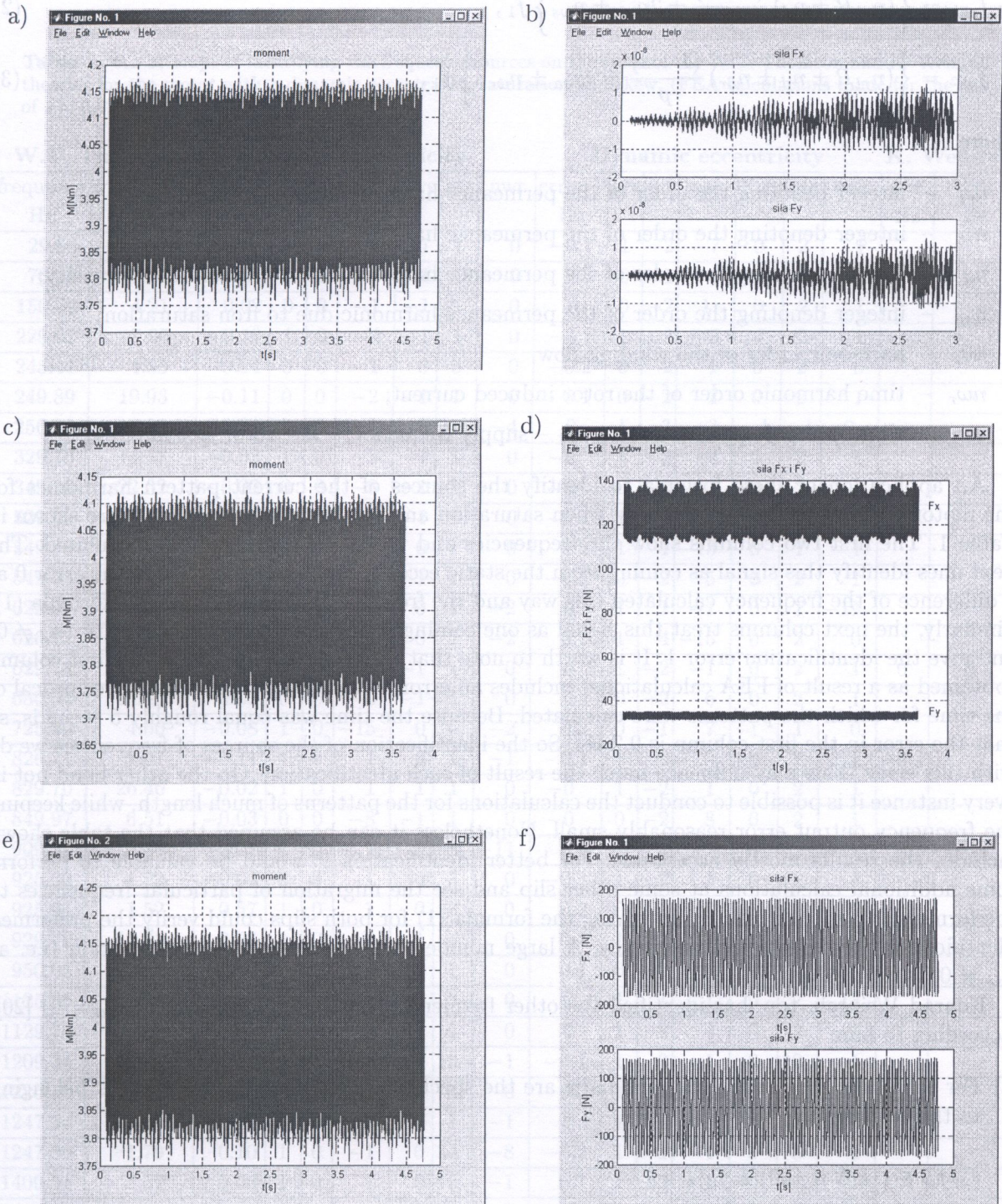


Fig. 8. Typical results of calculations of torques and  $F_x$  and  $F_y$  forces in time domain using the FEA model: a) torque b) forces in the motor free of defects c) torque d) forces in the motor with static eccentricity e) torque f) forces in the motor with dynamic eccentricity

The stator current frequencies can be predicted on the basis of the W.T. Thomson theory [17, 18, 19]:

$$f_{sh^1} = \left\{ (n_{rt}R \pm n_d) \frac{(1-s)}{p} \pm 2n_{sa} \pm n_{\omega_s} \right\} f_1, \quad (2)$$

$$f_{sh^2} = \left\{ (n_{rt}R \pm n_d \pm n_{\theta_r}) \frac{(1-s)}{p} \pm 2n_{sa} \pm n_{\omega_r s} \right\} f_1, \quad (3)$$

where

$n_{rt}$  – integer denoting the order of the permeance harmonic due to rotor slotting;

$n_{st}$  – integer denoting the order of the permeance harmonic due to stator slotting;

$n_d$  – integer denoting the order of the permeance harmonic due to dynamic eccentricity;

$n_{sa}$  – integer denoting the order of the permeance harmonic due to iron saturation;

$n_{\theta_r}$  – harmonic order of the winding flow;

$n_{\omega_r}$  – time harmonic order of the rotor induced current;

$s$  – slip;  $p$  – pole-pairs number;  $f_1$  – supply frequency;  $R$  – rotor slot number.

An application of these formula to identify the sources of the current pattern harmonics for the motor with a dynamic eccentricity when saturation and bar skew are considered, are shown in Table 1. The first two columns show the frequencies and the signal magnitude as calculated. The next ones identify this signal as coming from the static eccentricity ( $n_d = 0$ ) and give the error 0 as a difference of the frequency calculated this way and the frequency calculated from the formula (1). Similarly, the next columns treat this signal as one coming from the dynamic eccentricity ( $n_d \neq 0$ ) and give the identification error 1. It is worth to note that the frequency shown in the first column (obtained as a result of FEA calculations) includes an error. It equals approximately a reciprocal of the time for which the patterns were calculated. Because the time was equal roughly 5 seconds, so that the error in the first column is 0.2 Hz. So the identification of the sources of frequencies we do with this error. This may influence much the result of such identification. On the other hand not in every instance it is possible to conduct the calculations for the patterns of much length, while keeping the frequency output error reasonably small. Nonetheless it can be assumed that the table shown includes the results mostly acceptable. For better identification it would be valuable to perform some additional calculations at some other slip and see the migration of particular frequencies to the formula (1) in both results. Satisfying the formula (1) for both slips could verify the preformed identification for a particular frequency. A large number of frequencies due to saturation (i.e. at  $n_{sa} \neq 0$ ) is noticeable.

Konrad Weinreb, too, has identified the other frequencies not due to saturation ( $n_{sa} = 0$ ) [20]. According to him:

- a) For the static eccentricity characteristic are the spectrum components of frequencies belonging to the set where

$$f_{st} \in \{(k N n / 60) \pm f_o\}_{k=1,2\dots}$$

where  $N$  – rotor slot number,  $n$  – speed,  $f_1$  – supply frequency.

- b) For the dynamic eccentricity characteristic are the spectrum components of frequencies belonging to the set where

$$f_d \in \{(k 2 p n / 60) \pm f_o\}_{k=1,2\dots}$$

**Table 1.** An attempt of identifying the frequency sources on the basis of the W.T. Thomson and K. Weinreb theories for the motor with a dynamic eccentricity, saturation and skew. (FEA calculations made for the slip of  $s = 0.0289$ )

W.T. Thomson			Static eccentricity						Dynamic eccentricity						K. Weinreb		
frequency Hz	magnitude dB	error 0 Hz	nrt	nd	nsa	nws	ntr	nwr	error 1 Hz	nrt	nd	nsa	Nws	ntr	nwr	stat Hz	dyn Hz
29.66	12.48	-0.06	1	0	-6	-1	1	0	-0.1	1	-2	-7	0	2	1		
70.21	5.97	-0.07	1	0	-7	-1	1	0	0.3	0	1	0	0	1	-2		
150.02	4.21	0.02	0	0	-1	-1	1	0	0	0	-2	1	0	2	1		
229.62	7.66	-0.10	1	0	-4	-1	1	0	-0.1	1	-2	-5	0	2	1		
245.41	4.35	-0.24	0	0	1	0	3	0	-0.2	0	2	1	0	2	0		
249.89	19.93	-0.11	0	0	-2	-1	1	0	-0.1	0	-2	2	0	2	1		
256.93	1.82	-0.31	0	0	-3	0	1	-4	0	1	-3	-3	-1	1	0		
329.70	13.57	-0.02	1	0	-3	-1	1	0	-0	1	-2	-4	0	2	1		
349.98	22.32	-0.02	0	0	-3	-1	1	0	-0	0	-2	3	0	2	1		
529.66	15.41	-0.06	1	0	-1	-1	1	0	-0.1	1	-4	-1	0	1	-1		
549.08	4.17	0.53	0	0	5	0	1	0	0.2	1	1	-13	0	1	-1		
549.93	12.93	-0.07	0	0	-5	-1	1	0	-0.1	0	-2	5	0	2	1		
625.05	3.42	-0.33	1	0	-1	0	1	-2	0	1	1	-1	0	1	-19		
626.12	6.19	0.05	1	0	-14	0	2	-2	0.1	1	4	-15	0	2	0		
629.74	25.07	0.02	1	0	0	-1	1	0	0	1	-2	-1	0	2	1	0	0
650.02	11.13	0.02	0	0	-6	-1	1	0	0	0	-2	6	0	2	1		
725.99	4.66	-0.08	1	0	-15	0	2	-2	0.3	0	-1	7	1	1	0		
826.71	2.07	-0.11	1	0	1	0	1	-1	-0.1	1	2	0	0	2	1	-0.1	
829.70	26.46	-0.02	1	0	1	1	1	0	-0	1	-2	1	0	2	1		
849.97	6.51	-0.03	0	0	-8	-1	1	0	-0	0	-2	8	0	2	1		
909.51	2.38	0.07	1	0	1	0	3	-11	0.1	1	2	1	0	2	-11		
925.30	1.72	-0.07	1	0	1	0	3	0	-0.1	1	2	1	0	2	0		
925.94	1.52	0.57	1	0	1	0	3	0	0.2	0	-1	9	1	1	0		
929.79	17.93	0.06	1	0	2	1	1	0	0.1	1	-2	2	0	2	1		
950.06	2.90	0.06	0	0	-9	-1	1	0	0.1	0	-2	9	0	2	1		
1125.05	15.82	-0.33	1	0	3	0	3	0	0	1	1	1	0	7	-13		
1129.74	9.52	0.02	1	0	4	1	1	0	0	1	-2	4	0	2	1		
1209.34	3.84	-0.11	1	0	-1	0	13	-1	-0.1	1	2	-1	0	12	-1		
1225.13	16.56	-0.25	1	0	4	0	3	0	-0.3	1	2	4	0	2	0		
1247.54	1.80	0.43	0	0	12	0	1	-1	0	1	1	0	0	12	-27		
1247.96	1.79	0.10	1	0	-1	0	14	-8	-0.2	1	1	4	0	3	-1		
1409.51	5.57	0.06	1	0	1	0	13	-1	0.1	1	2	1	0	12	-1	0.1	0.1
1425.09	1.75	-0.29	1	0	6	0	3	0	0.1	1	1	-2	0	19	-1		
1509.38	7.26	-0.07	1	0	1	0	15	1	-0.1	1	2	1	0	14	1		

- c) For the mixed eccentricity (which is the result of joint occurrence of static and dynamic eccentricity) characteristic are the spectrum components of frequencies belonging to the set where

$$f_m \in \{|k(n/60) \pm f_o|\}_{k=1,2...} \setminus \{f_{st}\} \setminus \{f_d\}. \tag{2}$$

- d) The harmonic components of frequencies typical for a motor with a symmetrical airgap can be recognized in the spectrum. They belong to the set where

$$f_{sym} \in \{(k g N n / 60) \pm f_o\}_{k=1,2...} \quad f_{sym} \in \{\{f_{st}\} \wedge \{f_d\}\}.$$

The set of those frequencies is the intersection of the frequency sets proper for static and dynamic eccentricities.

In Table 2 a frequency identification according to the above formula has been made splitting them into two columns: the “stat” suffix identifies the ones due to static eccentricity and the “dyn” suffix, due to dynamic eccentricity. When performing the above calculations it is important to preliminary define the speed of rotation of the rotor. The frequencies which differ by  $2f_1$  Hz are noticeable in Table 2. These differences are due to the term  $\pm f_1$  which is present in the above formulae. They can be used to define the speed of rotation.

If the speed of  $n_1$  equals to  $n_2$  then we can assume that it is calculated rotor speed of rotation.

**Table 2.** Some examples of defining the speed from the harmonics measurements when the eccentricity occurs

• static	• dynamic	• symmetrical airgap
N=28; f0=50; k=1;	p=2; f0=50.; k=1;	g=1; N=28; f0=50; k=1;
fst1=4434.38;	fdyn1=2142.19;	fsym1=1144.78;
fst2=4334.38;	fdyn2=2042.19;	fsym2=1044.78;
n1=(fst1-f0)*60./(N*k)	n1=(fdyn1-f0)*60./(2*k*p)	n1=(fsym1-f0)*60./(g*N*k)
n2=(fst2+f0)*60./(N*k)	n2=(fdyn2+f0)*60./(2*k*p)	n2=(fsym2+f0)*60./(g*N*k)

### 7. FEA METHOD TO MEASUREMENT RESULTS COMPARISON FOR A MOTOR WITH BROKEN BAR

Measurements have been made with MOTORMONITOR program:

Spectral lines at frequencies of  $(1 - 2s)f_1$  and  $(1 - 4s)f_1$  which appear when defects are present, can be noticed (Fig. 9). The same frequencies appear in the results of calculations performed on the mathematical model of the induction motor using FEA method, which has been described in this paper.

### 8. IDENTIFICATION OF FREQUENCIES IN THE STATOR CURRENT SPECTRUM

To verify the calculations measurements have been made for the motor with dynamic eccentricity and the results has been collected in the Table 4. A frequency range of 500 Hz through 5 kHz has been taken into account for the measurements (pattern filtering). For both the measurements and the calculations the slip of  $s = 0.0289$  has been maintained.

By using the formula (1), the following frequencies can be defined,

for $n_{sa} = 0$ and $n_{ws} = 1$			for $n_{sa} = 1$ and $n_{ws} = 1$			for $n_{sa} = -1$ and $n_{ws} = 1$		
$n_d = 0$	$n_d = -1$	$n_d = 1$	$n_d = 0$	$n_d = -1$	$n_d = 1$	$n_d = 0$	$n_d = -1$	$n_d = 1$
729.77	705.49	754.05	829.77	805.49	854.05	629.77	605.49	654.05

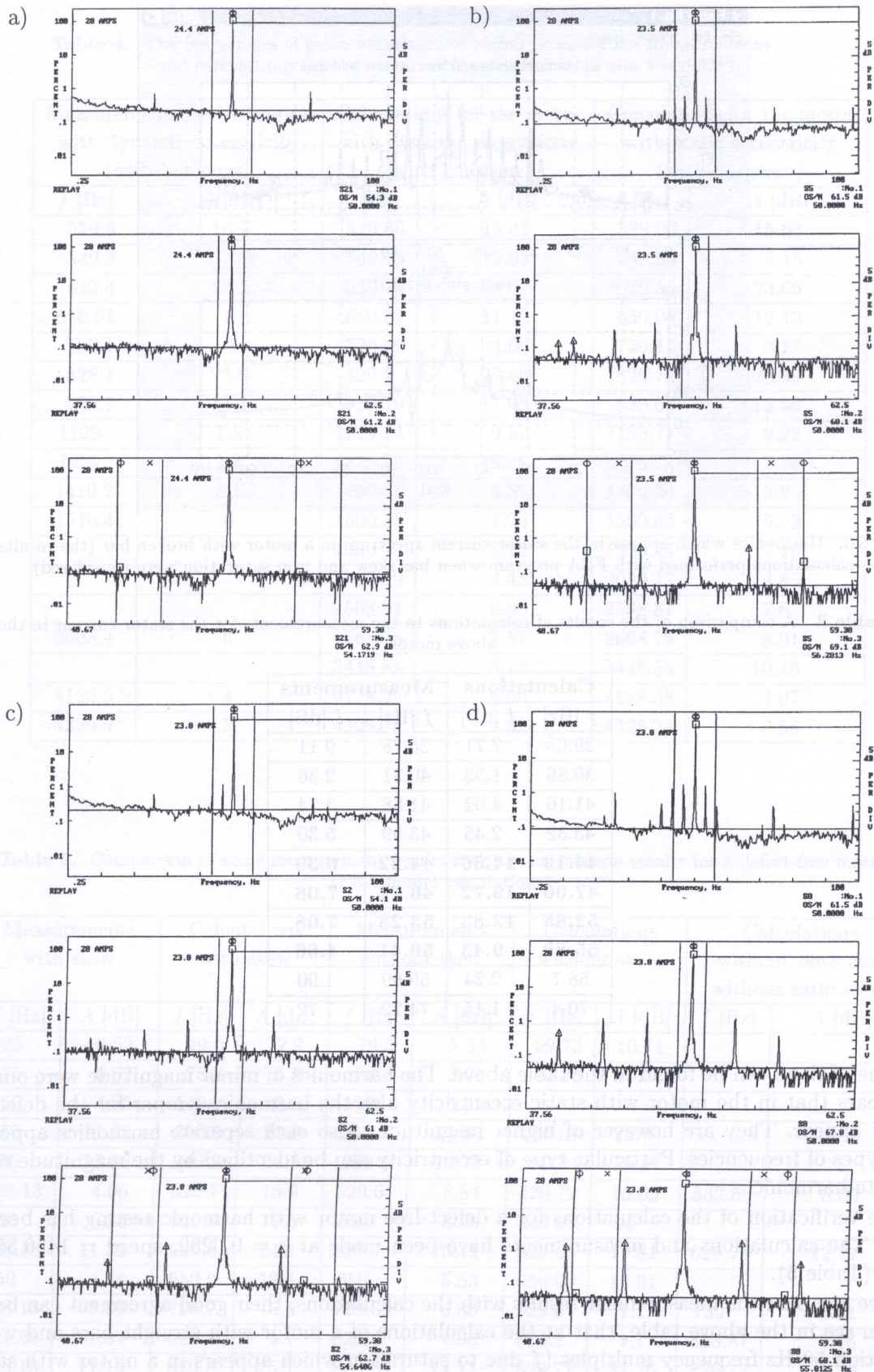
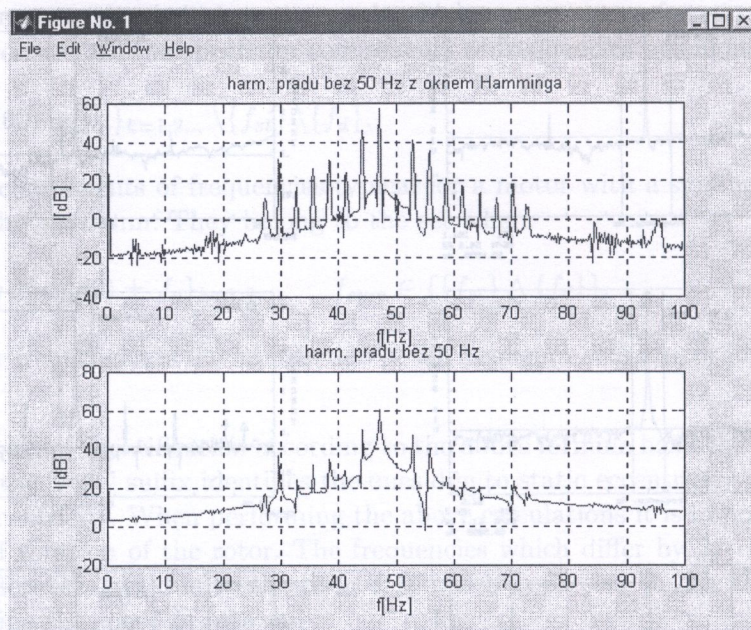


Fig. 9. Stator current measurements with MOTORMONITOR program for a) a defect-free motor, b) a motor with broken bar, c) a motor with broken ring, d) a motor with broken bar and ring



**Fig. 10.** Harmonics which appear in the stator current spectrum in a motor with broken bar (the results of calculations performed with FEA program when bar skew and iron saturation were considered)

**Table 3.** A comparison of the results of calculations to the measurements for the stator current in the above motor

Calculations		Measurements	
$f$ [Hz]	$I$ [dB]	$f$ [Hz]	$I$ [dB]
29.68	7.71	25.78	9.11
39.86	1.53	40.31	2.36
41.16	4.02	41.88	3.74
43.32	2.45	43.59	5.30
<b>44.19</b>	<b>14.56</b>	<b>44.22</b>	<b>6.39</b>
<b>47.00</b>	<b>19.72</b>	<b>46.72</b>	<b>7.08</b>
<b>52.85</b>	<b>12.83</b>	<b>53.28</b>	<b>7.08</b>
<b>55.89</b>	<b>9.43</b>	<b>56.41</b>	<b>4.66</b>
58.7	2.24	59.69	1.90
70.4	1.15	74.22	7.72

Some of them can be found in the table above. The harmonics of minor magnitude were omitted. It appears that in the motor with static eccentricity also the harmonics proper for the defect-free motors appear. They are however of higher magnitude. Also each separate harmonics appear for both types of frequencies. Particular type of eccentricity can be identified by the magnitude of each separate harmonic.

The verification of the calculations for a defect-free motor with harmonic testing has been also made. The calculations and measurements have been made at  $s = 0.0289$ , speed = 1456.55,  $I = 2.65A$  (Table 5).

If we compare the measurement results with the calculations, their good agreement can be seen. We can see in the above table, that at the calculations of a motor with straight bars and without saturation 50 Hz frequency multiples ( $f$  due to saturation which appears in a motor with straight bars with saturation) do not appear. The differences in magnitudes are caused by the assumption of different signal cutoff level at calculations and measurements. They can be caused by some rotational speed fluctuations at measurements.

**Table 4.** The frequencies of some harmonics of higher order for the measurements and calculations for the motor with eccentricities at slip  $s = 0.0289$

Measurements for the motor with dynamic eccentricity (with bar skew)		Calculations for the motor with dynamic eccentricity (with bar skew)		Calculations for the motor with static eccentricity (with bar skew)	
$f$ [Hz]	$A$ [dB]	$f$ [Hz]	$A$ [dB]	$f$ [Hz]	$A$ [dB]
529.8	15.7	529.66	15.41	529.66	15.63
549.3	3	549.93	12.93	549.03	5.15
629.4	23.2	629.74	25.07	629.59	23.65
650.01	9	650.02	11.13	650.08	12.13
729.1	4	726.99	4.66	726.14	3.17
828.1	23.9	829.7	26.46	829.72	26.49
929.7	11.1	929.79	17.93	929.64	18.56
1129	1.8	1129.74	9.52	1129.77	9.22
1225	1.8	1225.13	16.56	1229.7	2.56
1410.2	8.1	1409.51	5.57	1409.34	5.95
1510.4	6	1509.38	7.26	1509.55	6.03
		1989.1	8.12	1989.24	7.18
		2089.19	4.48	2089.17	4.85
		2568.91	6.98	2568.87	7.6
2668.4	6	2668.78	7.57	2668.79	8.01
		3448.88	3.77	3448.55	10.48
4129.9	4	4128.25	5.06	4128.38	4.07
4329.9	3	4328.18	2.62	4328.23	3.56

**Table 5.** Comparison of some measurement results with the calculation results for a defect-free motor (FEA model calculations)

Measurements with skew		Calculations with skew		Measurements without skew		Calculations without skew		Calculations without skew and without saturation	
$f$ [Hz]	$A$ [dB]	$f$ [Hz]	$A$ [dB]	$f$ [Hz]	$A$ [dB]	$f$ [Hz]	$A$ [dB]	$f$ [Hz]	$A$ [dB]
25	6.62	29.6	12.2	26.5	5.53	29.73	10.71		
75	6.62	70.2	6.6	74.5	3.61	70.23	10.05		
150	4.85	149.9	3.5	150	5.21				
250	11.92	250.0	21.8	250	11.55	250.07	23.9		
350	13.56	349.9	21.3	350	14.75	350.04	15.4		
528.13	4.06	529.7	15.9	529.6	8.84	529.72	16.05	532.59	8.09
550	6.85	549.9	11.5	550	8.05	549.97	14		
628.13	11.22	629.8	24.1	629.7	13.11	629.68	17.81	629.79	22.27
650	4.48	650.0	12.1	650	5.53	650.09	13.91		
728.13	3.09	726.7	5.1	729.69	6.86	729.6	1.1	730	0.01
821.88	1.84	821.8	4.1	823.4	1.06	823.1	1.1	823.87	9.16
828.13	11.14	829.8	25.7	829.69	14.11	829.77	31.76	826.77	5.29
928.13	2.1	929.7	18.5	929.69	2.7	929.73	24.22		

**Table 6.** Some results obtained from the calculation performed with FEA method for the induction motor under consideration (slip  $s = 0.0289$ , skew and iron saturation taken into account)

defect-free		with dynamic eccentricity		with static eccentricity		without saturation and with straight bars	
$f$ [Hz]	$A$ [dB]	$f$ [Hz]	$A$ [dB]	$f$ [Hz]	$A$ [dB]	$f$ [Hz]	$A$ [dB]
27.3	1.3	27.32	0.98	27.23	2.76	153.86	4.19
27.9	0.5	29.66	12.48	29.75	13.11	180.67	4.93
29.6	12.2	70.21	5.97	70.17	5.73	234.55	0.99
70.2	6.6	150.02	4.21	72.98	0.15	280.91	5.47
149.9	3.5	229.62	7.66	149.89	3.28	342.05	1.23
229.6	7.5	240.5	0.37	229.6	8.14	411.71	1.61
245.3	1.3	242.42	1.31	245.32	4.46	433.76	0.05
250	21.8	243.06	1.69	250.09	20.95	511.7	2.8
253.9	1	243.49	1.98	256.27	3.35	534	1.58
255	0.1	245.41	4.35	261.32	0.92	546.03	3.26

**Table 7.** Seeking frequencies and magnitudes obtained from the calculations (measurements can be also used) for the motors with static and dynamic eccentricity

Both eccentricities occur		Only one eccentricity occurs	
Dynamic	Static	Dynamic	Static
$f$ [Hz]	$f$ [Hz]	$f$ [Hz]	$f$ [Hz]
27.32	27.23	240.5	72.98
29.66	29.75	242.42	261.32
70.21	70.17	243.06	262.44
150.02	149.89	243.49	263.85
229.62	229.6	257.79	325.88
245.41	245.32	258.21	345.53
249.89	250.09	620.35	449.1
329.7	329.81	638.92	602.92
349.98	350.02	639.56	603.48
529.66	529.66	639.99	604.6
545.45	545.38	826.71	610.78
549.08	549.03	925.94	613.87
925.3	924.87		2868.92
929.79	929.64		4673.19

To find some characteristic frequencies for a given defect the procedure shown in the Tables 6 and 7 can be proposed.

The next step is to compare the frequencies already selected for given type of eccentricity with the frequencies obtained for the defect-free motor. So we can find the frequencies (and their magnitudes) which are characteristic for the particular eccentricity. Such comparison has to be made not only separately for the calculations or measurements but first of all between them.

## 9. COMPUTATIONAL MODEL 3D DESCRIPTION

In addition to the static forces resulting from the engine operation to produce the driving torque, also dynamic forces act upon the rotor of the electric motor. These forces are due to the



mechanical and electrical motor features. The mechanical forces result from the rotor unbalance allowances or damages to the elements of rotor bearings. The forces of the magneto-electric origin are due among the others to the change of the length of the airgap between the rotor and stator caused by their misalignment. The alternating forces generated in the rotor can be amplified when to the frequencies of the free vibration of the rotor-stator unit. Thus it is important to know the distribution of the free vibration frequencies for the whole unit. To determine the risky areas of the motor operation it is necessary to perform the calculations of the free vibration frequencies for the whole unit. In the model presented here the rotor shaft complete with core plates and the cage winding. Additionally the model includes also the housing parts complete with two covers, stator core plates and winding elements. The bearings placed in the stator covers were modelled with elastic elements having the appropriate elasticity. Values for the free vibration of such model were determined with finite elements method. The rotor geometry was modelled in the MSC/PATRAN system. To determine the eigen values ABAQUS v5.8 program was used. The calculations were performed in the Academy Computer Center in Cracow, Poland.

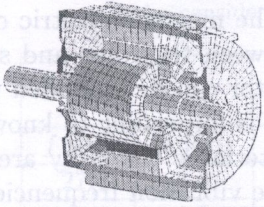
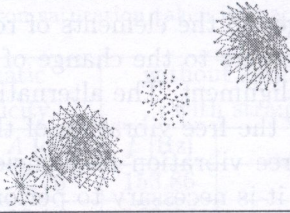
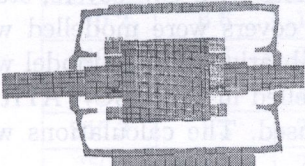
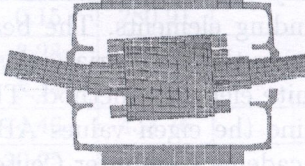
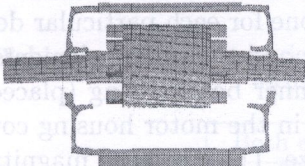
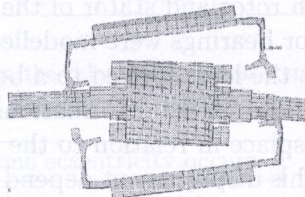
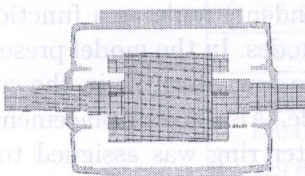
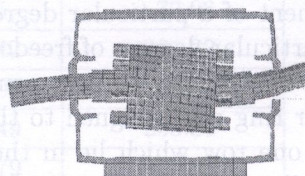
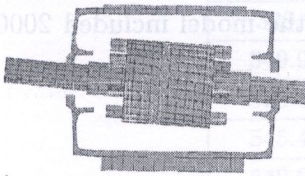
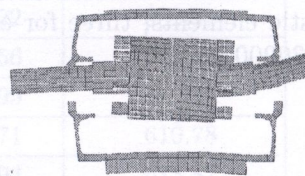
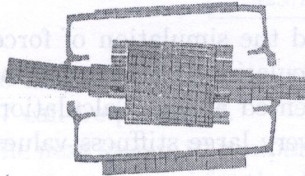
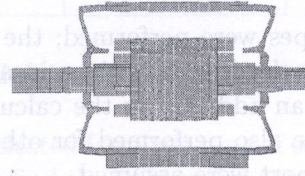
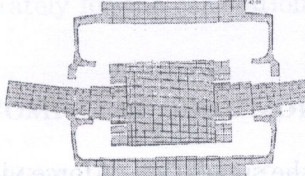
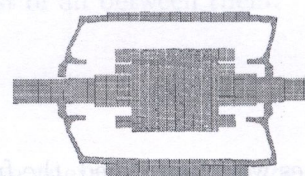
Elements of various types were used to build the FE mesh. They were mostly eight- or six-node solid elements. Both rotor and stator of the electric motor were modelled with such elements. Each one of the both rotor bearings were modelled with 3 spring elements (one for each particular degree of freedom). Due to the load applied to a bearing, the bearing raceway and the rolling elements are subject to deformation. These deformations cause the center of the inner bearing ring (placed on the shaft pin) to displace in relation to the outer bearing ring (placed in the motor housing cover). The magnitude of this displacement depend on the bearing type and size. The displaced magnitudes can be determined with empirical relations. Appropriate MPC Explicite type elements were used to connect the spring elements to the stator and bearing cover. These elements give the option to express a displacement of a particular degree of freedom of one (dependent) node as a function of displacements of particular degrees of freedom of other (independent) nodes. In the model presented here the arithmetic average for displacements of the shaft nodes of one row which lie in the center of the bearing inner ring was assigned to the displacement of one node. Also the displacements of the shaft nodes of one row which lie in the center of the bearing outer ring was assigned to the second node in similar fashion (these are also appropriate nodes from the bearing seat bored in the cover). An elastic element which links the shaft to the housing was placed between these two nodes. A separate elastic element was created to for each degree of freedom. This resulted in 6 MPC elements and e elastic elements, three for each bearing. Additionally the model included 20000 of solid elements and 30000 nodes.

## 10. ANALYSIS

Analyses of two types were performed; the free vibration analysis and the simulation of force vibration. To analyse the free vibrations in a more detailed fashion calculations of the rotor model were performed as an addition to the calculations for the model presented above. Calculations of the rotor alone were also performed for other form of its support. A very large stiffness values for the rotor shaft support were assumed.

### 10.1. Free vibration analysis

Analyses of two types were performed, the free vibration analysis and the simulation of force vibration.

	Bearing stiffness $K = 37313$	Bearing stiffness $K = 24055$		Boundary condition	
				$f$ [Hz]	$f$ [Hz]
	510.0	453.6		2081.0 2085.6	2050.6 2051.9
	591.5 602.8	506.0 512.0		2755.5	2710.8
	650.8	650.0		3576.0 3592.0	3572.4 3581.5
	870.8 971.8	775.1 829.0		3847.6	3758.1
	1336.6	1251.0		4081.0	3783.8
	1677.1	1664.4		4111.0	3819.0

## 10.2. Forced vibration analysis

Forced vibrations has been simulated by the application of the direct integration method. An input has been, in the form of a concentrated forces, applied in several locations on the shaft. They acted at various frequencies. All these analyses referred to an electric motor so simulated to include motor casing as well as all elastic machine elements. To solve the problem a function acting during 20 periods at the sampling frequency of 1/10 the period.

## 11. CONCLUSIONS

1. The torsional vibration frequency remains practically invariant for various computational models and is 655 Hz for the rotor model with rigid support in RTZ system and 650.8 Hz for the model of the whole motor with the rotor supported flexibly in the motor case.
2. The traverse rotor vibrations change according to the model type. The highest flexural frequency shows the model with rotor shaft rigidly supported and it is 2043.8 Hz in RTZ system, for the model with MPC elements and rigid support it drops down to 1368 Hz, and to 667.6 Hz when elastic rotor support is taken into account (bearing stiffness 37313 N/mm) and if motor casing with covers is considered in the model the frequency drops down to the value close to 600 Hz. It can be seen that in the most developed model the first flexural frequency is almost three times lower than in RTZ model. Considering the bearing and motor case flexibility leads to the development of simple flexural form of the shaft vibrations. In a developed model of the motor the flexural forms of the vibrations of the shaft superimpose over the displacements of the bearing shaft supports as well as bearing covers displacements, which creates even more complex flexural forms of the shaft vibrations.
3. It can be seen that in the transverse vibrations at 602.8 Hz the major share has the bearing support stiffness. It is worth to note that the displacements on both supports are in the same phase, but at the 870.8 Hz frequency the displacements in the bearing supports are in counter-phase. At the frequency of 1336 Hz also the displacements in the motor casing add up to the overall displacements. At the 1667 Hz frequency displacements of the shaft alone and in the shaft supports are in counter-phase to the displacements of the case. At the frequency of 3576 Hz the rotor shaft vibrates at II harmonic. At frequencies of 1667, 4081.7, 4111 Hz the share of the case vibrations becomes more prominent, and at 2775.5 Hz – the rotor vibrations.
4. After the consideration of various electric motor models one can come to the conclusion that taking into account that shaft support conditions which closer to the actual ones decreases significantly free vibration frequencies and develops even more complex rotor vibration forms.
5. Forced vibration calculations performed with the direct integration and modal analysis methods. The case when input is effected by gyrating force applied in the rotor center of gravity. The simulations of the vibrations influenced by the rotor unbalance have shown that both static and dynamic displacements obtained during the analysis were the same. It seems that the dynamic boost influence is insignificant.
6. Forced vibrations analysis. The simulations of the bearing failure in the right support have shown that the displacement of the free shaft end is two times greater than the shaft displacement for the location where the load is applied. In the case of direct integration they are almost 4 times greater than the static displacements. There occurs such significant increase in the dynamic displacements occurs because the input frequency is very close to free form vibration frequency of the system.

We had 15 motors for the testing in our disposal. These were:

- without any defects,
- with straight bars,
- with static eccentricity,
- with dynamic eccentricity,
- with broken bar, with broken ring and both defects present.

The defects under considerations were purposely factory-introduced. The calculations were performed at the slip of  $s = 0.0289$  and with the eccentricity  $e = f = 0.00007$  m. It would be interesting to investigate the relation between the stator current harmonics and the presence of neutral line. The differences between the measurements and calculations are caused by speed fluctuations during the measurements. At static eccentricity the speed fluctuations were small but at the dynamic one they were more noticeable. From the formula (1) at the identification of harmonics, the differences in frequencies caused by the term of  $n_{wr}sf = n_{wr}1.45$  can be seen.

According to [17] the static eccentricity in general does not cause new frequencies to form as compared to the defect-free motor; it only increases their magnitudes. The dynamic eccentricity however creates new frequencies according to (1). They are shifted as compared to the previous ones by the term of  $\pm n_d(1-s)/p f_1$ . Among the stator current harmonics there are many created by the iron saturation. However the more significant are those frequencies, which are not due to saturation. Only such frequencies are considered in [20]. Much more frequencies appear when straight bars are present. Their magnitudes are greater than those, which appear when there are skewed bars. Both the skew and saturation have damping effect to the amplitudes.

It would be interesting to estimate more accurately the influence of the eccentricity level at different eccentricity types at both measurements and calculations.

The long time of induction motor calculations with the FEA method influenced also the long time of the computer operation. So, for the computation purpose, emerges the idea to use much faster reluctance-network model. If we only get the same frequencies, then it could substitute the FEA model, e.g. for the calculation of the parametric relations. This will be subject of further studies.

## REFERENCES

- [1] A. Arkio. Unbalanced pull in a high-speed induction motor with an eccentric rotor. *ICEM'94*.
- [2] J.L. Coulomb. A methodology for determination of global electromechanical quantities from a finite element analysis and its application to the evaluation of magnetic forces, torques and stiffness, *IEEE Trans. Magn.*, **19**: 2514–2519, November 1983.
- [3] M. Dąbrowski. *Projektowanie Maszyn Elektrycznych Prądu Przemiennej*. Warszawa, 1988.
- [4] L. Gołębiowski. *Residualne Modele Maszyn Elektrycznych*. Rzeszów, 1996.
- [5] T. Glinka. Diagnostics of the winding insulation of electrical machines using a constant voltage. *Electrical Technology Russia*, **1**: 31–37, ZNACK, Russia, 1998.
- [6] G. Kamiński, W. Przyborowski. *Uzwojenia i Parametry Maszyn Elektrycznych*. Oficyna Wydawnicza PW, Warszawa, 1998.
- [7] K. Kluszczyński. *Momenty Pasożytnicze w Indukcyjnych Silnikach Klatkowych*. PTETiS. Warszawa–Gliwice, 1993.
- [8] M. Noga, L. Gołębiowski, D. Mazur. Calculation of rotor defects of the induction motor using FEM. *HIPER'98*, October 14–16, 1998, Zurich, Switzerland.
- [9] K. Pawluk, T. Schweitzer. Application of magnetic field analysis methods to calculations of electric machines. *Przegląd Elektrotechniczny*, **72**(8): 193–199, 1996.
- [10] J. Penman, A. Stavrou. Broken rotor bars: their effect on the transient performance of induction machines. *IEE Proceedings. Electric Power Applications*, **143**(6): 449–457, Nov. 1996.
- [11] W. Rams, J. Rusek, J. Skwarczyński. Forces acting on induction machine stator core due to winding faults. *Archiv für Elektrotechnik*, **76**(3): 219–224, 1993.

- [12] J. Rusek. Reflection of eccentricities in spectral composition of currents of induction machines. *ICEM96 Proceedings. International Conference on Electrical Machines*. vol. 2, 470–475, Univ. Vigo, Spain 1996.
- [13] J. Rusek, J. Skwarczyński. Symulacje komputerowe niesymetrii klatki wirnika silnika indukcyjnego. *Kwartalnik Elektrotechnika*, **10**(4): 385–400. AGH, Kraków 1991.
- [14] S.J. Salon. *Finite Element Analysis of Electrical Machines*. Kluwer Academic Publishers, Boston–London–Dordrecht, 1995.
- [15] T. Sobczyk, A. Warzecha, P. Drozdowski, K. Weinreb, J. Mikulik. *Modelowanie Matematyczne Zjawisk Elektromagnetycznych w Maszynach Elektrycznych*, monografia 169. Kraków, 1994.
- [16] T. Śliwiński, A. Głowacki. *Parametry Rozruchowe Silników Indukcyjnych*. PWN, Warszawa, 1982.
- [17] W.T. Thomson, A. Barbour. On-line current monitoring and application of a finite element method to predict the level of static airgap eccentricity in three-phase induction motors. *IEEE Transactions on Energy Conversion*, **13**(4): 347–357, Dec. 1998.
- [18] W.T. Thomson, A. Barbour. Finite element study of rotor slot designs with respect to current monitoring for detecting static airgap eccentricity in squirrel-cage induction motors. *IAS '97*.
- [19] W.T. Thomson, J.R. Cameron, A.B. Dow. Vibration and current monitoring for detecting airgap eccentricity in large induction motors. *IEE Proceedings – B Electric Power Applications*, **133**(3): 155–163, May 1986.
- [20] K. Weinreb, J. Petryna, T. Węgiel. Analiza porównawcza wyników obliczeń i pomiarów wybranych przypadków ekscentryczności maszyn asynchronicznych. *Materiał sprawozdawczy Instytutu Elektromechanicznych Przemian Energii Politechniki Krakowskiej*, 1995.
- [21] S. Williamson. Induction motor model using finite elements. *Proc. ICEM, I*, 1–8, 1994.
- [22] A. Witkowski. *Zastosowanie Diagnostyczne Modeli Matematycznych Silnika Indukcyjnego Bazującego na Wyznaczeniu Indukcyjności Metodą Permeancji Międzyzębowych*. Praca doktorska. Gliwice, 1997.

## 1. INTRODUCTION

Algorithms for solving global optimization problems can be classified into heuristic methods that find the global optimum only with high probability, and methods that guarantee to find a global optimum with some accuracy. An important class belonging to the former type are the stochastic methods [20]. A number of techniques such as simulated annealing [26] and genetic algorithms [10] use analogies to physics and biology to approach the global optimum. The most important class of methods of the second type are branch and bound methods [11]. They originate from combinatorial optimization, where global optima are also wanted but the variables are discrete and take several values only. Branch and bound methods guarantee to find a global optimum with a desired accuracy after a predictable (though often exponential) number of steps. The basic idea is that the configuration space is split repeatedly by branching into smaller and smaller parts. This is not done homogeneously, but instead some parts are preferred and others are eliminated. The details depend on bounding procedures. Lower bounds on the objective allow to eliminate large portions of the configuration space early in the computation so that only a (usually small) part of the branching tree has to be generated and processed. The lower bounds may be obtained using dc-method [25], techniques of the interval analysis [10, 23], or methods based on the knowledge of Lipschitz constants [19]. In many mechanical and civil engineering optimization problems, sensitivity and gradient methods are applied [2, 8, 15, 26]. If an objective function and constraints are differentiable, Kuhn-Tucker conditions can be applied [6]. Many references about optimization methods is available on the internet [27, 28].

In this paper, applications of the interval global optimization method [10–23] to the optimization problems in applied mechanics are considered. The method can also be applied to the following engineering problems:

- optimization of parameters of mechanical systems [4],
- shape optimization [21],
- calculation of extreme values of mechanical system [20].